Towards using harmonic “contamination” as signal for thin reflectors

Christopher B. Harrison, Gary Margrave, Michael Lamoureux, Arthur Siewert, Andrew Barrett and J. Helen Isaac

ABSTRACT

Vibroseis is currently the favoured source used for seismic land acquisition where conditions permit. A pilot signal generates a sweep of designed length and frequency range which drives the vibrator to impart a signal into the earth. Due to non-linearity in the vibrator hydraulics and mechanical systems, as well as near surface non-linearities, higher order harmonics of the pilot signal are generated, “contaminating” both sweep and the seismic record. Traditionally these higher order harmonics have been targets for attenuation during acquisition and processing. In 2011 CREWES and POTSI developed algorithms to decompose these harmonics within a “contaminated” vibrator sweep. In this paper we explore the use of these decomposed harmonics for bandwidth expansion for better imaging of thin beds.

Introduction

Harmonic contamination of seismic data acquired using a vibrator is a well known phenomenon. The harmonics occur due to non-linearities in the vibrator mechanisms (Walker 1995; Wei 2011) and non-linearities in the near surface (Lebedev 2004). Many techniques have been developed which attempt to attenuate these harmonics during acquisition (Silverman 1979; Rozemond 1996; Moerig 2004; Bagaini 2006; Benabentos 2006; Bagaini 2010; Abd El-Aal 2011) and the processing phase (Sorkin 1972; Eisner 1974; Rietsch 1981; Schrodt 1987; Martin 1989; Okaya 1992; Martin 1993; Li 1995; Walker 1995; Li 1997; Polom 1997; Dal Moro 2007; Abd El-Aal 2011).

In 2011 CREWES and POTSI developed an algorithm to decompose a harmonically contaminated vibrator sweep into its harmonic components. Harrison et al. (2011) used the Gabor transform and least squares methodology to successfully decompose a sweep from the first (H1) to eighth (H8) harmonic. Due to the Gabor transform providing a complex-value time-frequency spectrum of the sweeps, two separate methods for decomposition were developed. The first is time dependant Gabor decomposition (TDGD), which decomposes a sweep with respect to time, and the second method is the frequency dependant Gabor decomposition (FDGD) which decomposes a sweep with respect to its namesake. Harrison et al. (2011), at the time, were unsure as to which method, either TDGD or FDGD, produced better harmonic component results.

As stated above, higher order harmonics have traditionally been seen as noise to be attenuated out of both sweep and seismic data. The standard correlation process uses the pilot sweep for correlation which is band limited, unlike the harmonically “contaminated” sweep and traces. This desire to attenuate the harmonics is due to the correlation process causing ghost forerunners or a tail at both positive and negative correlations times (Seriff 1970). Successful harmonic decomposition of contaminated sweeps now provides a set of new operators for correlation purposes. The higher order harmonics have higher frequencies, which, as will be shown below with ideal conditions, when used as correlation operators, resolve thinner beds.

Finally, we are pleased to inform the reader that we have decided on a nomenclature alteration since the 2011 CREWES report. Admittedly, it is far easier to refer modes of vibration in terms of H1, as the fundamental AND as the first harmonic followed by H2 as the second harmonic, and so on, than it is to call the first harmonic, H2, second harmonic H3, etc. It is hoped that this taxonomy change from the previous 2011 CREWES paper will be more helpful when discussing harmonics.

Harmonic Decomposition

The test sweep used by Harrison et al. (2011) is reproduced in Figure 1 in time (top), frequency (middle) and Gabor (bottom) domains. This test sweep was taken from a 2D seismic survey conducted in September 2009 on a dirt road that had been iced down (water sprayed on the surface in temperatures well below zero degrees Celsius) in northern Alberta, Canada (Harrison et al., 2011). The road was iced for transportation purposes and allowed the vibrator to couple more efficiently with the surface of the earth. This particular sweep, 3801, was chosen based on its high signal-to-noise (S/N) ratio. A roll off at approximately 80% of Nyqist (800 Hz) can be observed on the Gabor (bottom) plot on Figure 1. This was done to facilitate harmonics due to filtering within the recorder.

Harrison et al. (2011) implemented both TDGD and FDGD to decompose the sweep shown in Figure 1 from the fundamental or first (H1) to the eighth harmonic (H8). A compact version of the TDGD and FDGD results of that decomposition is shown in Figure 2. For brevity, only the original sweep (black, Orig.), analyzed sweep (Anlz), H1+H2, H1, H2, H3 and H4 are presented in Figure 2 for both TDGD and FDGD. The H1+H2 is the combination of the first harmonic and second harmonics, which will be tested as a correlation operator.

Both the time and frequency plots in Figure 2 show several important differences between TDGD and FDGD. The most striking difference is that the decibel limits of the harmonic components in the frequency domain for TDGD are considerably lower, approximately 100 dbs, than the decibel limits of the FDGD. This lower decibel value gives each of the TDGD harmonics sharper frequency boundaries than the FDGD harmonics. However, the FDGD appears to "fill in" the original sweep better in the time domain, especially in the first three seconds of the sweep. It is unclear at this stage which of the two methods has superior decomposition ability. We will show below, however, the “sharper” frequency limits seen in TDGD could be the contributing factor to TDGD producing “stronger” RMS strength and better correlation results.

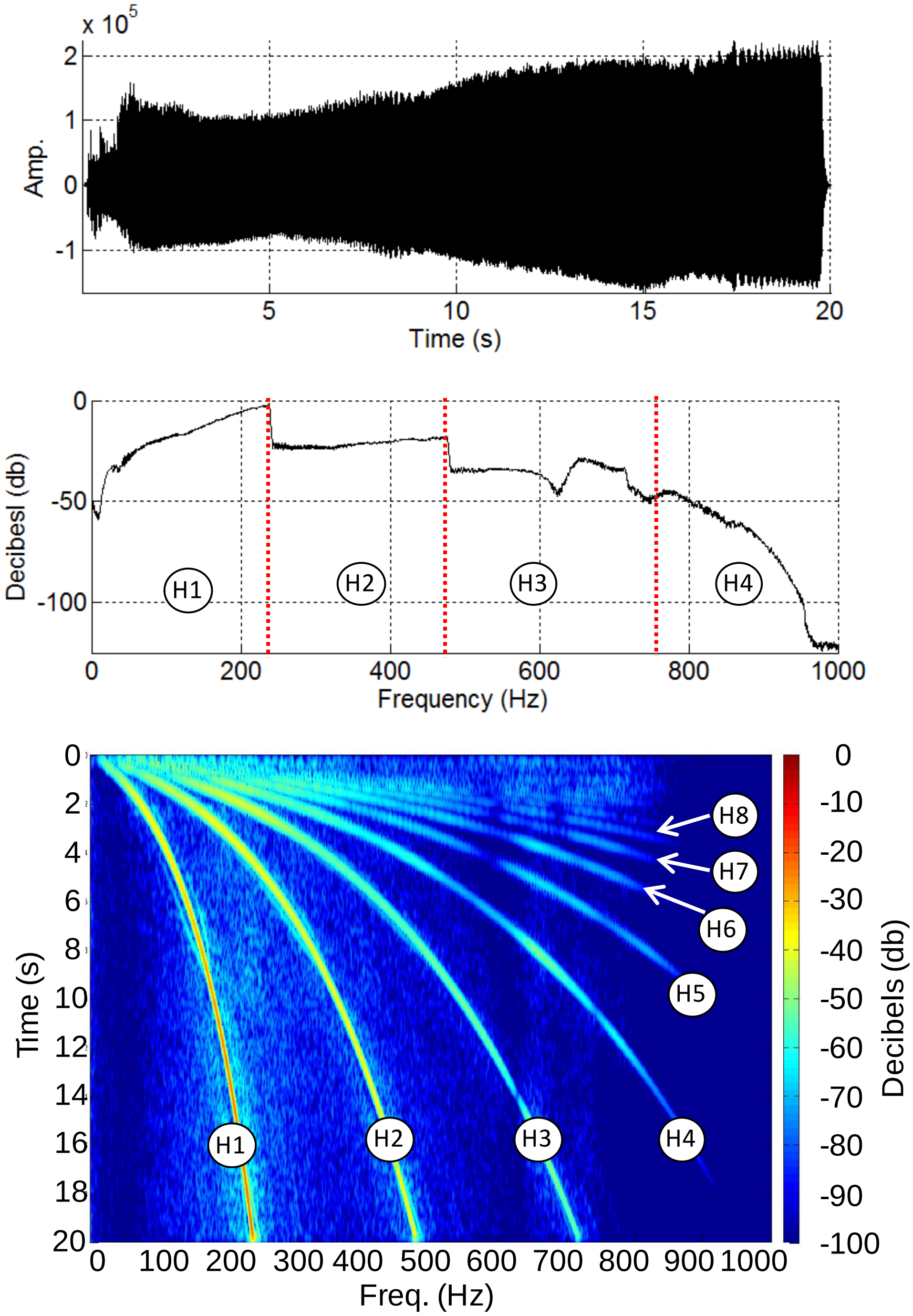

Figure 1. Sweep 3801 selected by Harrison et al. (2011) in time (top), frequency (middle) and Gabor (bottom) domains.

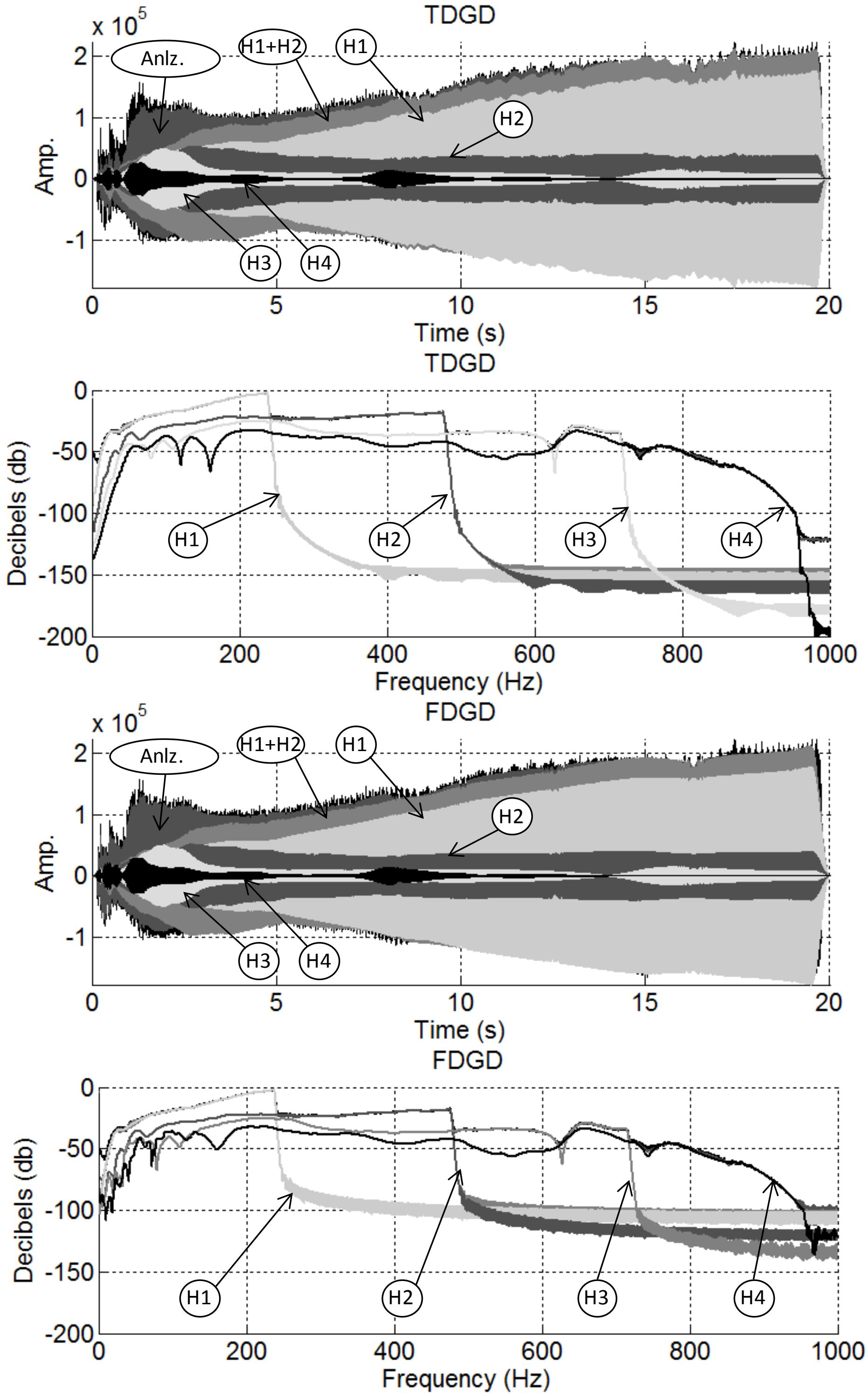

Figure 2. The results for TDGD and FDGD of the sweep 3801. The original sweep is plotted behind the harmonic results in black.

Harmonic Power

Successful decomposition of a single sweep from H1 to H8 was shown by Harrison et al. (2011) and reproduced in Figure 2. However, a single sweep does not a survey make. The survey from which the original test sweep was gleaned consisted of 1877 sweep points. Each of these sweep locations had three separate records for its respective sweeps. These separate records include the sweep recorded at the baseplate, the sweep recorded at the reaction mass, and the ground force. The baseplate and reaction mass are physical recording locations on the vibrator while the ground force is a “weighted-sum” calculation of the accelerations of the baseplate and the reaction mass based on a simplified linear model of oscillating masses, springs and dashpots (Beresnev 2012). All three of these records provide a total of 5631 “sweeps” for decomposition.

These “sweep” records were decomposed using both TDGD and FDGF from H1 to H8. Harmonics from each record were further re-composed into analysed sweeps and subtracted from the original sweep at their respective sweep points, creating an error record. This error record can also be considered the noise at each shot point. A batch process was designed for the above calculations, producing a combined 90,096 harmonics, sweeps and error records for analysis! Parallel processing is, of course, suggested for such a large set of computations.

The root mean square (RMS) strength was chosen as the best metric to vet this large volume of data by assessing the comparative strength of each harmonic, analyzed sweep and error calculation. Results of RMS power calculations for the baseplate records (A), reaction mass records (B) and ground force records (C) are plotted in Figure 3. The RMS power for the original sweep is plotted in light grey, the analyzed sweep is plotted in black and H1 is plotted in blue. The RMS strength for these sweeps and components are almost coincident on Figure 3 for the baseplate, reaction mass, and ground force. The RMS power of harmonics H3 to H8 and error, are all close in power at the bottom of each plot on Figure 3. The “stand out” feature on Figure 3 is the RMS power of H2. H2 is well below the RMS power of the analyzed sweep and H1, but noticeably above the RMS power of H3 to H8 and error.

Several more trends can be seen within RMS data shown in Figure 3. The variability in the baseplate and the reaction mass appear to compensate one another in the ground force, as seen between sweep points 1551 and 1301. Large spikes in error appear to coincide with power spikes of the original sweep and H1 in both baseplate and reaction mass records. Scales were re-plotted in Figure 4 between sweep points 1601 and 3201 to provide a more detailed view of the RMS power between these recording points.

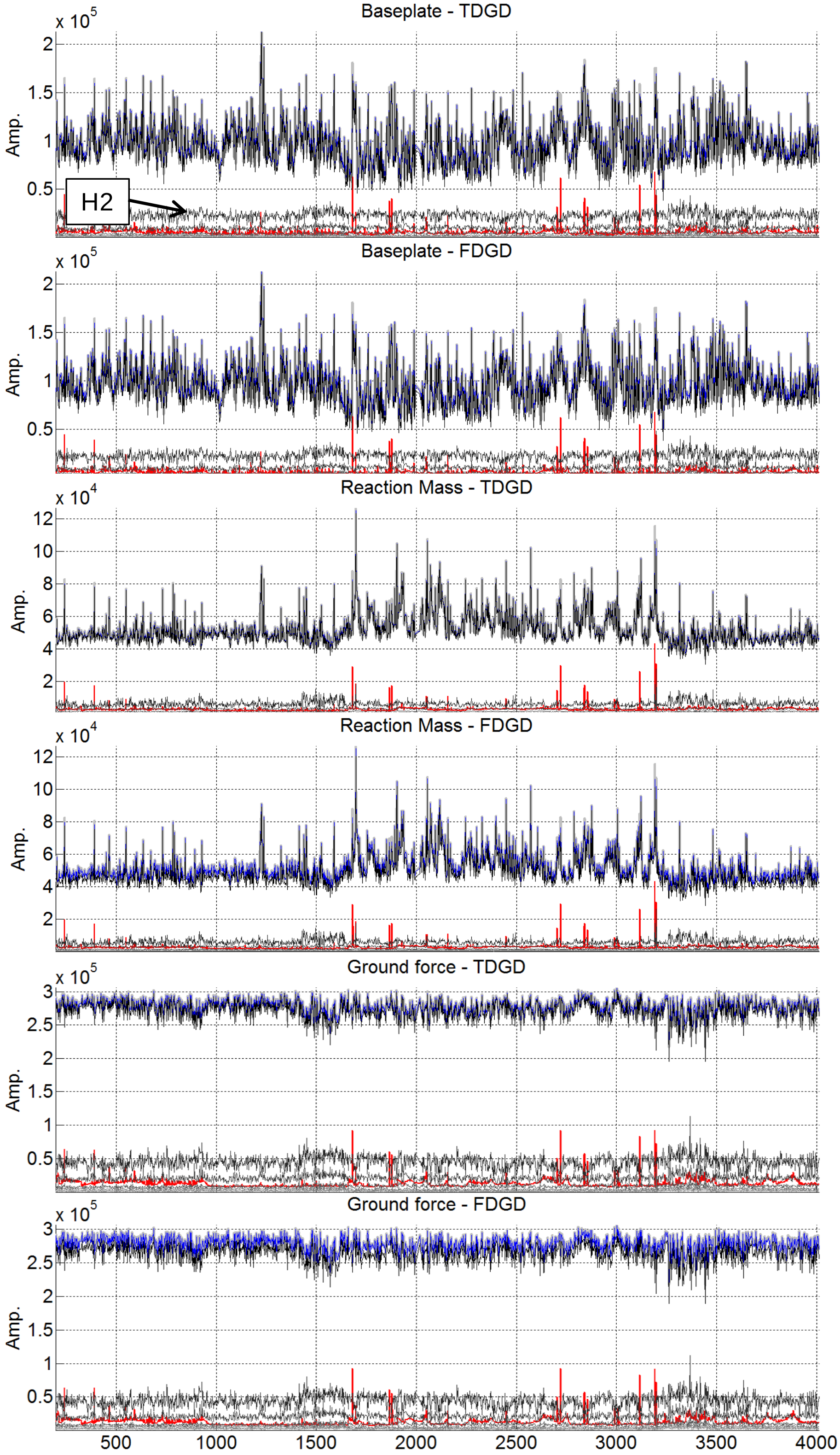

Figure 3. The RMS strength calculated at each shot point for the original sweep (light grey), analyzed sweep (black), and H1 (blue) for baseplate (A), reaction mass (B) and ground motion (C). H2 is indicated in black with H3 to H8 near the bottom. RMS strength of the error between the original sweep and the analyzed sweep is plotted in red.

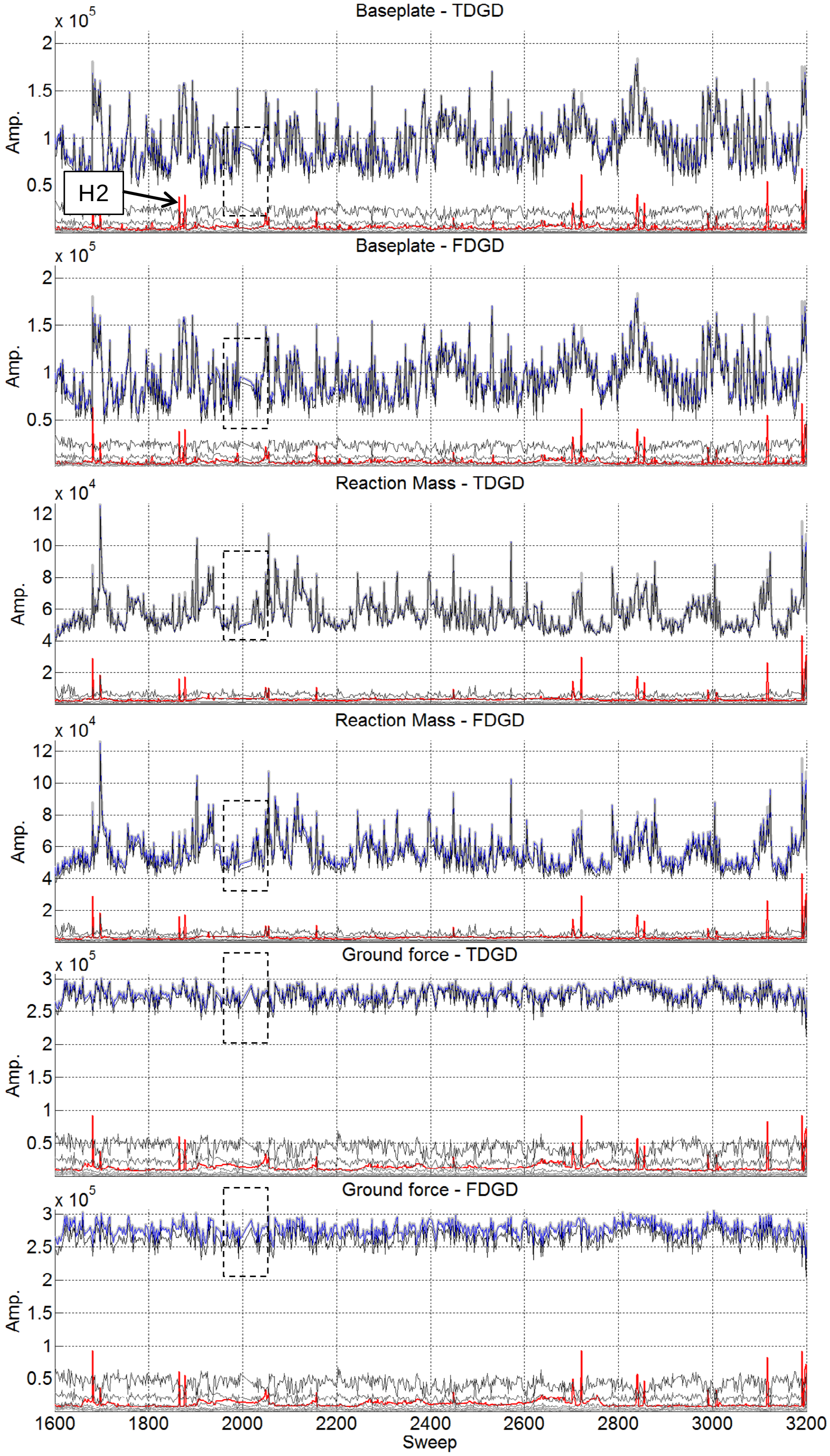

Figure 4. The RMS strength for each sweep point of the original sweep (light grey), analyzed sweep (black), H1 (blue) for the baseplate (A), reaction mass (B) and ground motion (C). H2 is indicated in black with H3 through H8 falling well below. The RMS strength of the error between the analyzed sweep and the original speed is plotted in red.

At the scale shown in Figure 4 we are able to see that RMS power of the noise (red) is near and in many cases exceeds the RMS power of harmonic components H3 to H8. Closer inspection shows that when error levels are high, presumably when noise levels are high, the error RMS power exceeds even that of the H2. A more significant observation is the RMS power differences between TDGD and FDGD seen between the baseplate (A), reaction mass (B) and ground force (B).

The dashed boxes on Figure 4 highlight a 6 shot gap in the recording line between shot point 1995 and 2019. The gap, in being graphed between these points, provides a convenient visual measure to observe the difference between RMS power of TDGD and FDGD. We can see that the RMS strength for TDGD is much closer (higher strength) to the RMS strength of the original sweep. However, the power differences between TDGD and FDGD appear to very small, in the order of single digit percentages. This small percentage could become significant in large surveys.

The error spikes as seen on Figure 4 stand out as points of interest as well. Four of these spikes located at 1681, 1980, 2157 and 2721, were selected to have their Gabor spectrums plotted. Figure 5 shows these error locations in decreasing RMS power value. Figure 4 shows that the RMS power of the error between the analyzed sweep and the original sweep could be used as shot point QC post acquisition to eliminated noisy sweeps.

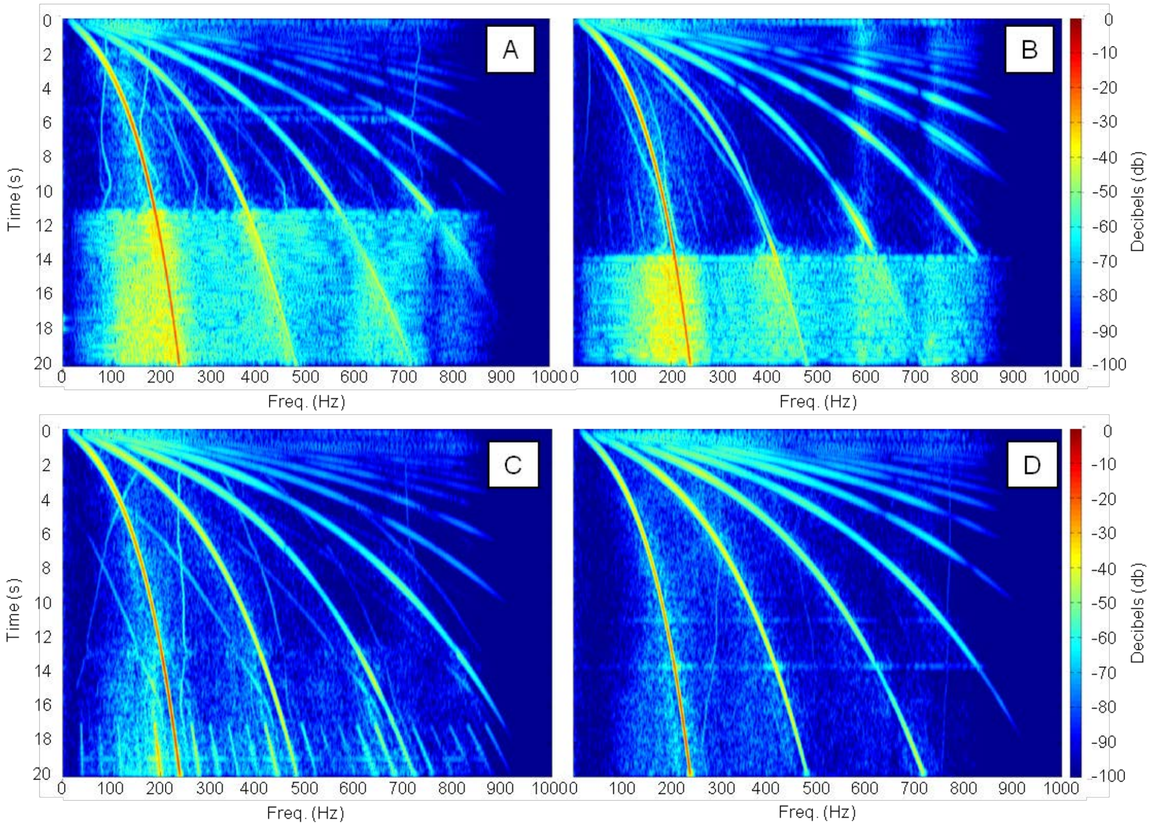

Figure 5. The Gabor spectrum of the baseplate recorded sweep at sweep point 1681 (A), 2721 (B), 2157 (C) and 1980 (D).

The RMS plots for all the original sweeps, analyzed sweeps, harmonics and error provided good insight into the relative signal strengths of all components present in this vibrator survey. The RMS power for H3 through to H8 in many cases did not exceed the RMS power of the error. This similarity in RMS strength may render H3 to H8 of little use for future correlation purposes. These harmonics may of course have other uses which can be explored in future research. H2, on the other hand, has an average RMS strength consistently above error RMS strength. This extra power, and sharper frequencies boundaries associated with H2 means that this component will be of keen interest as a correlation operator.

Application

We are now going to show that higher order harmonics can produce better resolution when imaging reflections. Three types of correlated data have been tested for their resolution ability. First we generated a non-linear synthetic sweep with harmonics from H1 to H4 using the pilot sweep equation for the vibrator used in the field survey referenced above. This synthetic sweep was then decomposed into its harmonic components using both TDGD and FDGD. A synthetic trace was generated by convolving the original synthetic non-linear sweep with a single spike reflectivity. A total of 12 correlations were calculated using TDGD and FDGD components to observe resolution capabilities of the decomposed harmonics and analyzed sweeps.

The second set of test data utilized the baseplate recorded sweep, 3801, from the field data supplied by StatOil. The decomposition of this particular sweep is covered by Harrison et al. (2011), and previously shown in Figure 2 above. This sweep was decomposed from H1 to H8 using both TDGD and FDGD. Synthetic traces were then calculated by convolving the original baseplate sweep with a single spike reflectivity, a three spike reflectivity, a 10 spike reflectivity, and a random reflectivity.

Finally, we tested the TDGD results to H2 on field data supplied by StatOil.

Non-linear Synthetic Sweep

The non-linear synthetic sweep for our first set of correlations tests was created using the pilot signal equation (1.1) below.

$$Fi(t) = Fb + \frac{Fe - Fb}{\log(\frac{1}{SegRa})} \times \log\left(1 + \frac{t}{T} \times (\frac{1}{SegRa} - 1)\right) \tag{1.1}$$

where

- SegRa = Sb/Se = $10^{(-Ra/10)}$
- Sb = Slope at the start of the log segment
- Se = Slope at the end of the log segment
- Fb = Start frequency

- Fe = End Frequency
- T = Te – Tb = Basic signal length
- Ra represents the attenuation (in dB) within the signal spectrum.

This pilot sweep equation was found in the Sercel VE464 vibroseis user manual (Sercel 2010). For the field data, Seismic Source Incorporated (SSI) electronic controls were used. This equipment controlled an 80% roll off which can readily be seen on Figure 1. While equation (1.1) does look complicated, it simplifies to a db logarithmic boost.

For brevity, only the fundamental (H1), second (H2), third (H3) and fourth (H4) harmonics were calculated and added together to created the final synthetic sweep. The amplitudes of each harmonic where chosen to best match the original amplitudes observed in the harmonic decomposition of the baseplate recorded sweep (Figure 2). Figure 6 shows the synthetic sweep in time (top), frequency (middle) and Gabor domains (bottom). This synthetic sweep was then decomposed using both TDGD and FDGD with the results shown in Figure 7. Decibel limits seen in Figure 7 are similar to the results of the baseplate recorded sweep seen in Figure 2. TDGD has lower decibel results than its FDGD counterpart, showing that TDGD may have an advantage over FDGD due to more pronounced frequency limits.

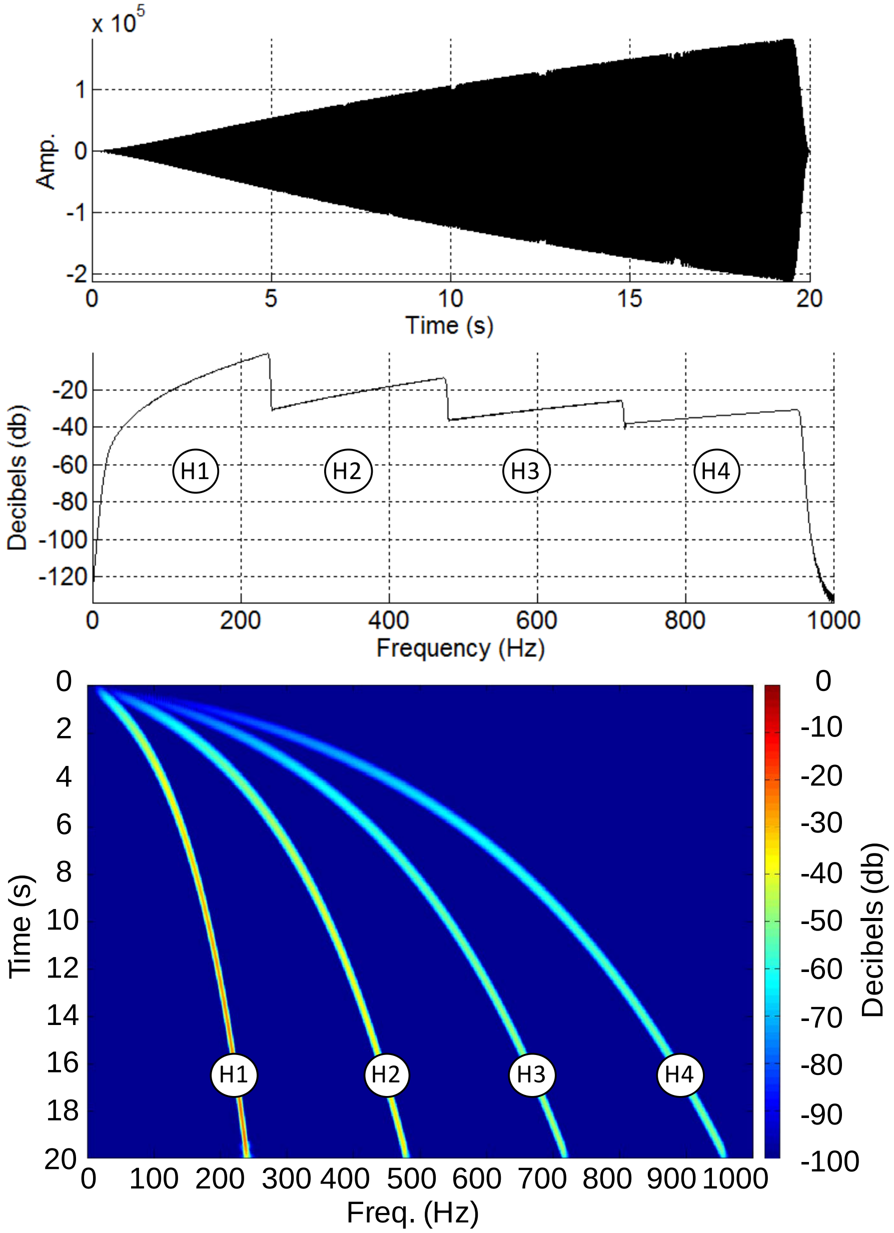

Figure 6. The time domain (B), frequency domain (C), and the Gabor domain for the synthetic sweep,

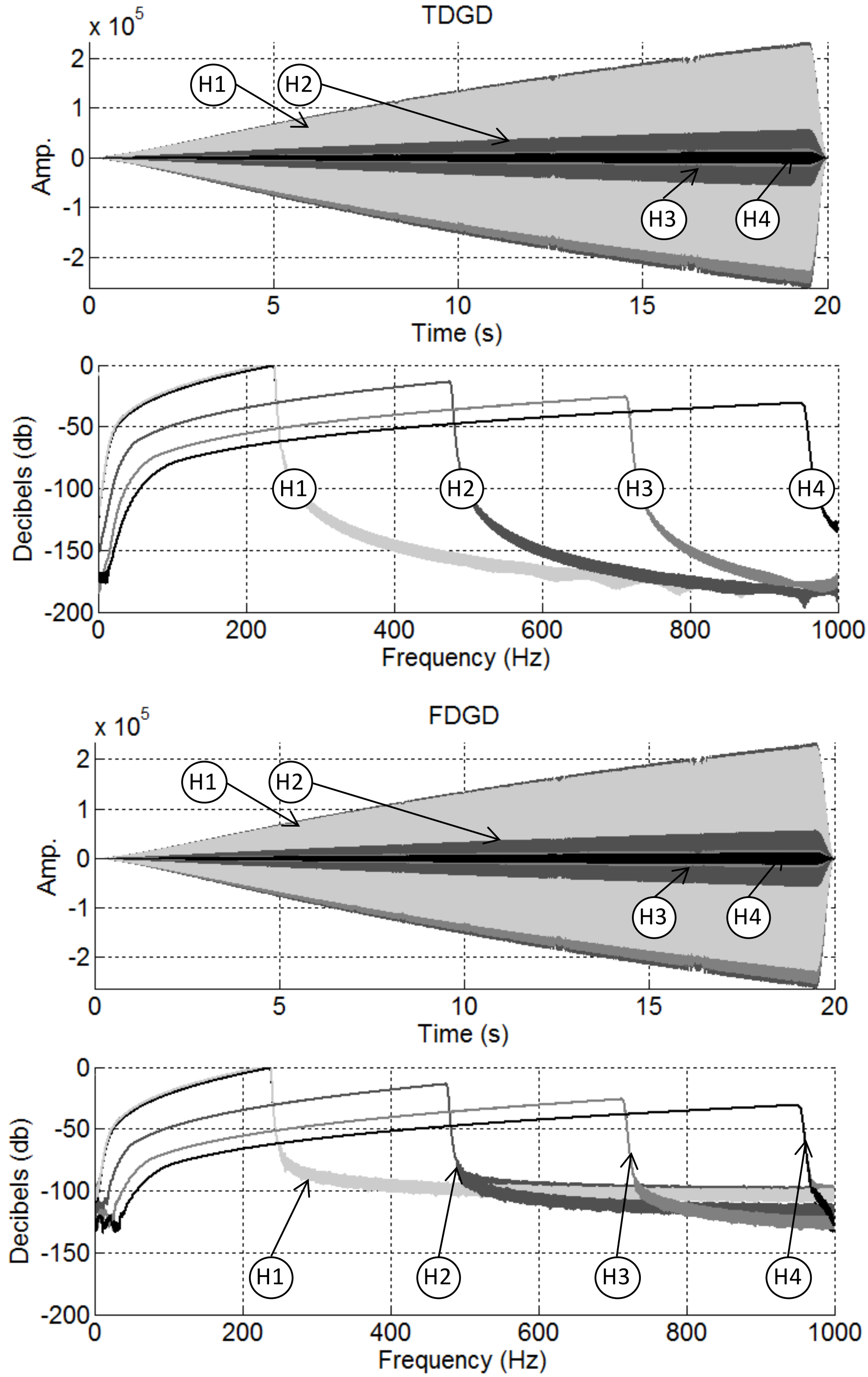

Figure 7. The TDGD (top) and FDGD (bottom) of the synthetic sweep shown in Figure 6.

Synthetic traces from non-linear sweeps

A single spike reflectivity was generated to convolve with the synthetic sweep seen in Figure 6. The reflectivity was designed to be 1 second long, have a sample rate of 0.5 ms (the same as the synthetic sweep) and amplitude of 0.2. Figure 8 shows the reflectivity (top), and the time domain comparison between the reflectivity and the synthetic sweep (middle). The amplitude of the reflectivity in Figure 8 (middle) has been scaled up for plotting purposes. The synthetic sweep was then convolved with the synthetic reflectivity and ready for correlation tests (bottom Figure 8). These convolution results will be called the synthetic traces and are free of spreading loss, noise and Q.

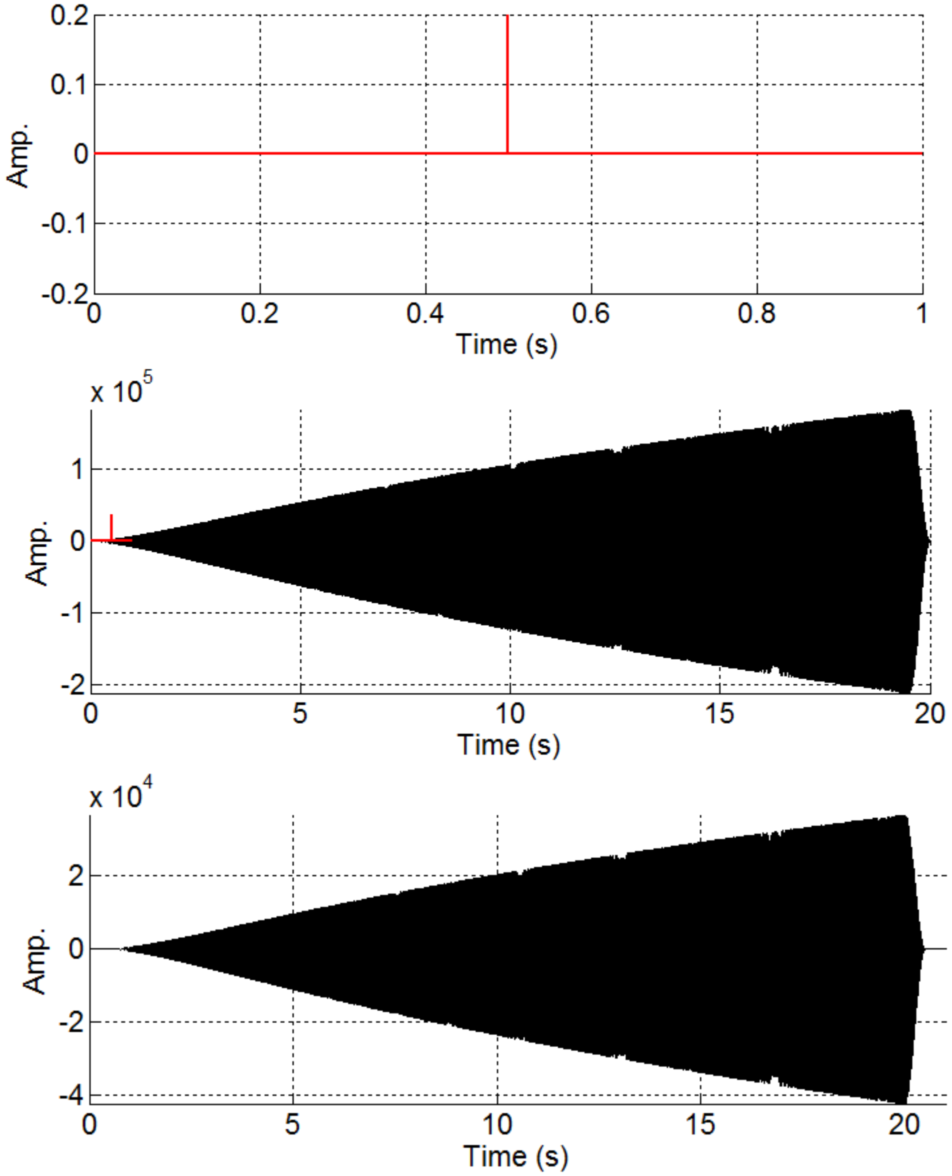

Figure 8. The single spike reflectivity (top), comparison of the synthetic reflectivity with the synthetic sweep (middle) and the result of convolving the reflectivity and the sweep (bottom).

Synthetic Correlations

A total of 12 correlations were conduction on the synthetic trace created from the convolution of a single spike reflectivity with a synthetic sweep. These correlations include the original synthetic sweep, the analyzed sweep, H1+H2, and H1, H2, H3 and H4 for both TDGD and FDGD. Figure 9 shows both TDGD and FDGD correlation results at two different scales. It is obvious from Figure 9 that subtleties in correlation differences between TDGD and FDGD will have to be imaged on an even smaller scale. A final scale change for these correlations is shown in Figure 10.

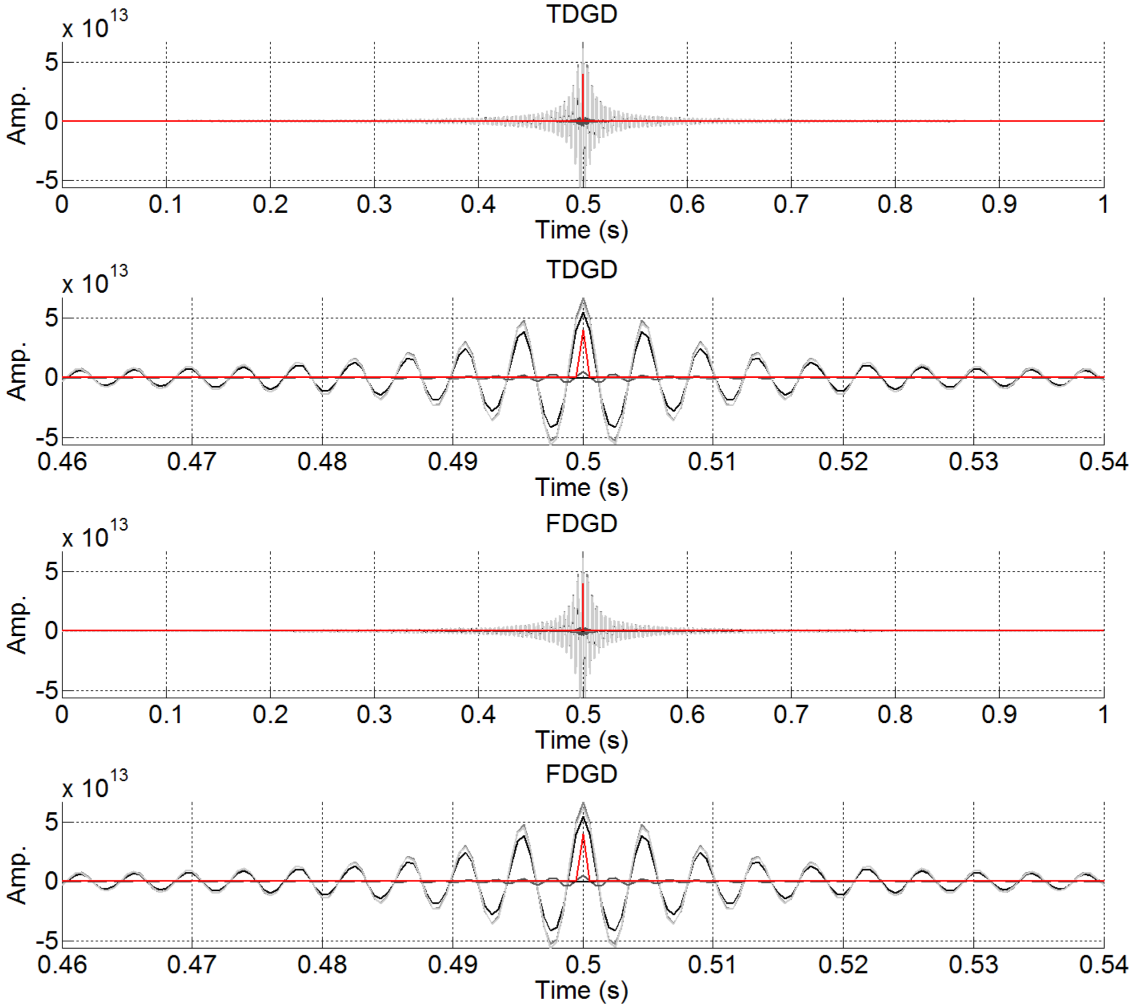

Figure 9. The correlation results for TDGD and FDGD utilizing original synthetic sweep, the analyzed sweep, H1+H2, and H1, H2, H3 and H4 for both TDGD and FDGD.

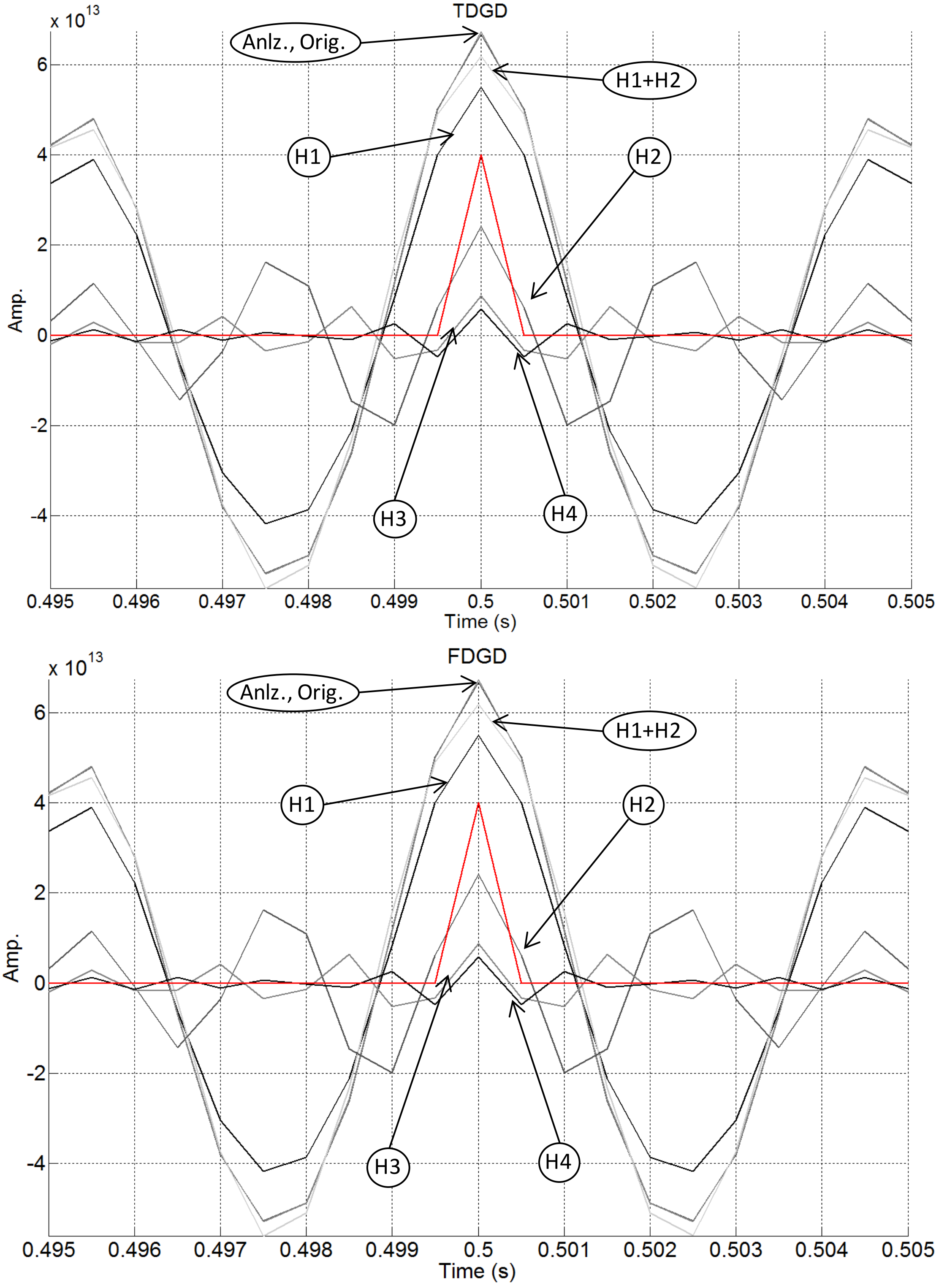

Figure 10. The correlation results of TDGD (top) and FDGD (botto) and a single spike trace.

Figure 10 reveals a more detailed image of the correlation results. The original synthetic sweep (Orig.) and the analyzed sweep (Anlz.) correlations are on top of each other in both TDGD and FDGD plots. H1+H2, represents the correlation of a sweep which combined the H1 and H2, and has higher amplitude than the correlation with just H1. The correlation for H2 was multiplied by 5, H3 was multiplied by 20, and H4 required a multiplier of 30 in order for their results to stand out on Figure 10. In this case, the correlation results show that H4 better resolves the spike than H3, which in turn better resolves the spike than H2. When all correlations from both TDGD and FDGD are superimposed on each other, there is no difference between either method in this single spike case.

Baseplate – Single spike reflectivity

The baseplate recorded sweep 3801 (Figure 1) was convolved with a single spike reflectivity exactly like the reflectivity shown in Figure 8 (top). For brevity, only the zoomed correlation of the original sweep (Orig.), analyzed sweep (Anlz.), H1+H2, and H1 to H4 for both TDGD and FDGD are shown in Figure 11. As was previously seen with regards to the synthetic sweep correlations in Figure 10, the analyzed sweep, the original sweep and H1+H2 correlations for sweep 3801 are almost identical. Further, just as in the case of Figure 10, H2 was multiplied by 5, H3 was multiplied by 20, and H4 required a multiplier of 30 in order for their results to stand out on Figure 11. What is new in the case of the baseplate correlations as compared to the synthetic sweep are the resolving differences between H2, H3 and H4.

In both the TDGD and the FDGD cases, H3 and H4 correlations do not appear to resolve the spike as well as H2 does on Figure 11. TDGD and FDGD correlations, excluding H3 and H4, were re-plotted Figure 12 to assess which decomposition method better resolved the single spike. In Figure 12 we can see from the inlaid image on left that correlations using TDGD components, while very small, have higher amplitude values than their FDGD counterparts. Zero crossing points for both TDGD and FDGD components appear to be near equal.

Looking back at the RMS power results in Figure 4 we see that TDGD components on average had more power than FDGD RMS values. With the higher amplitudes in correlation results and higher RMS power, the proverbial “scales” appear to be tipped in TDGD’s direction as the “best” decomposition method. While we will not completely disregard FDGD, for brevity we will only focus on TDGD for the remainder of this paper.

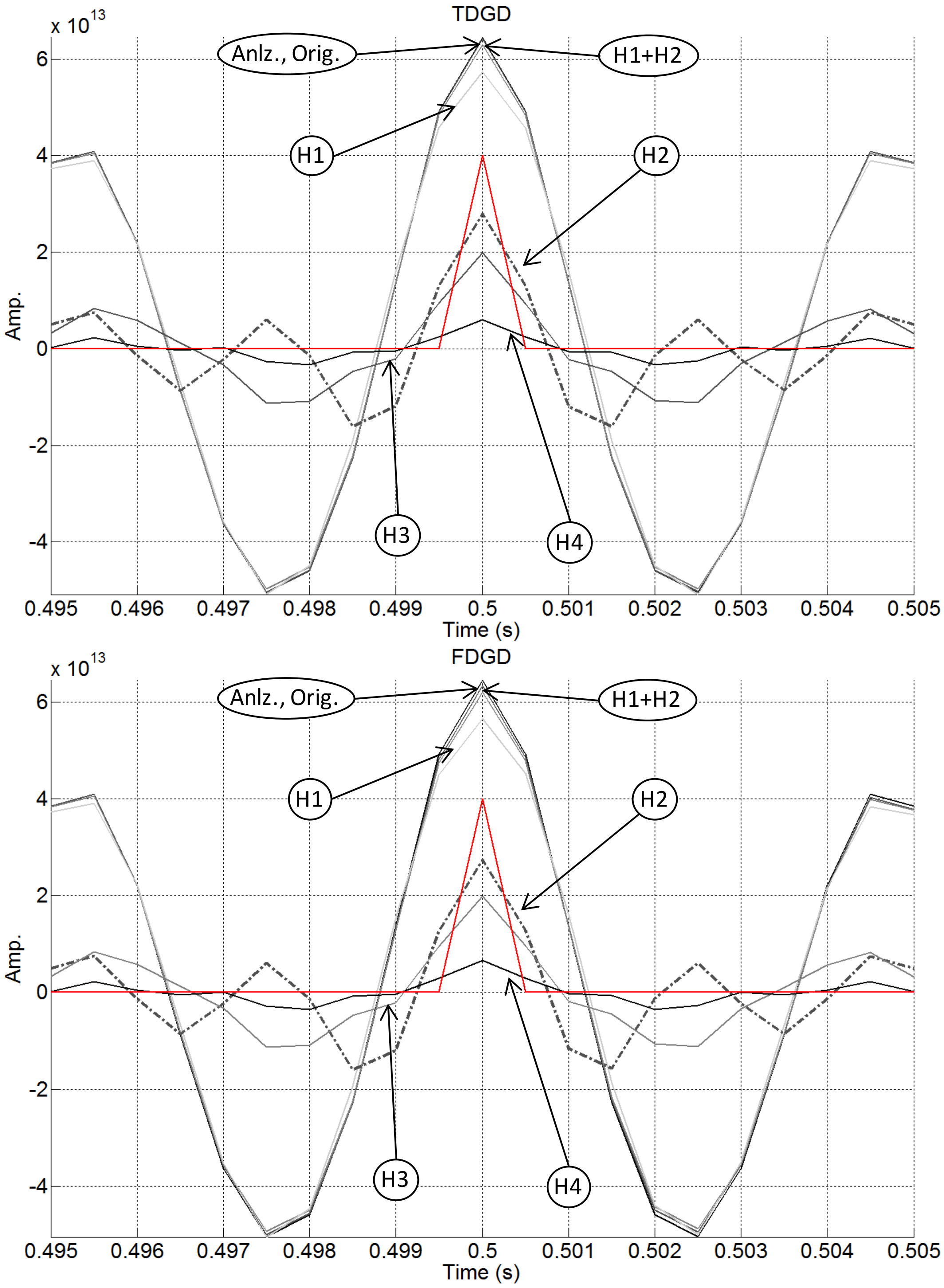

Figure 11. The correlation results of for TDGD (top) and FDGD (bottom) components from the baseplate record sweep at 3801 and a single spike trace.

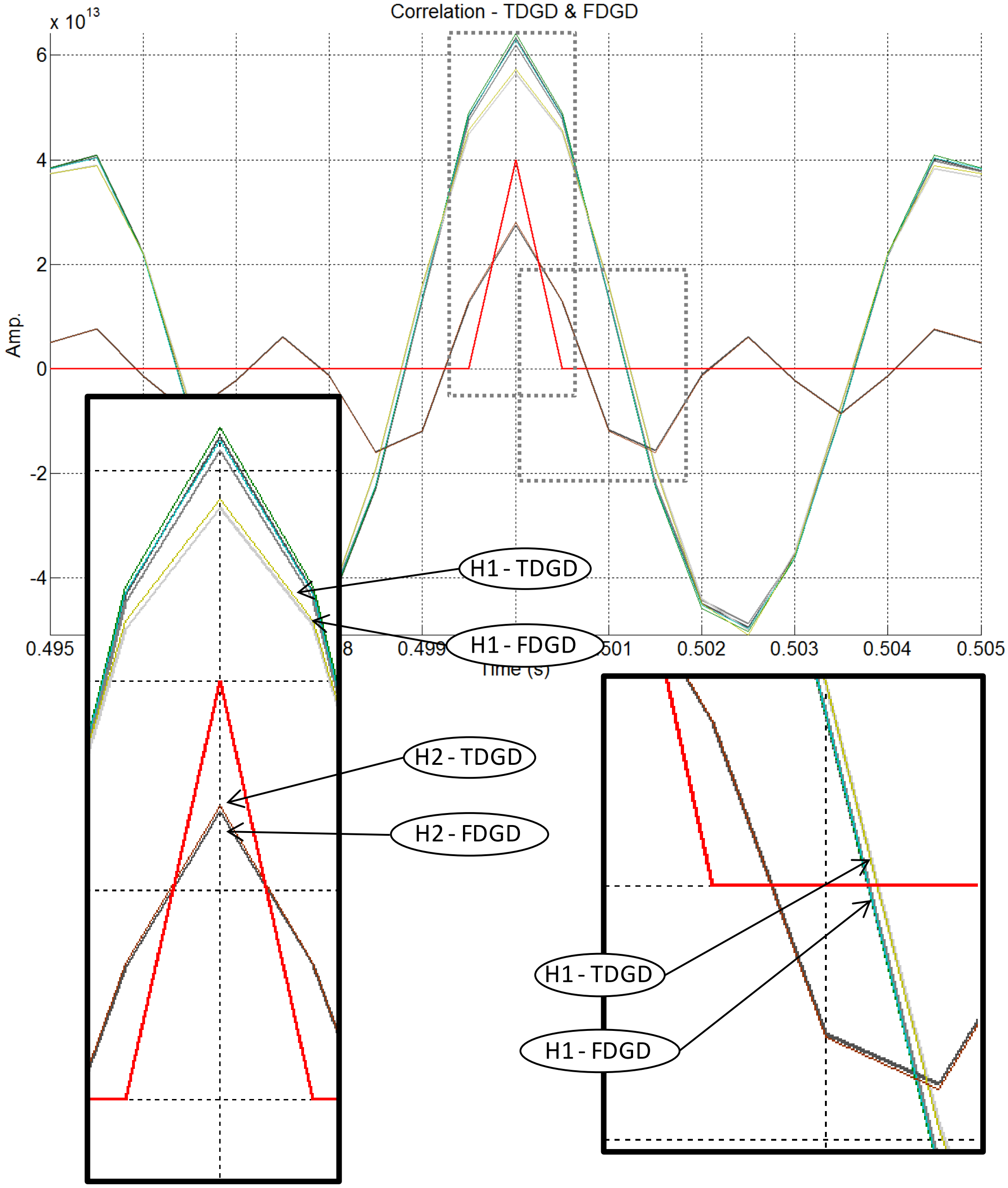

Figure 12. The combined TDGD and FDGD correlations with respect to the original, analyzed sweep, H1 and H2. Both inset images on the left and right correspond to the dotted box overlays on the main figure.

Baseplate – Multiple spike reflectivities

Three different reflectivities were generated to investigate the resolving power of TDGD components of sweep 3801. The first of the three reflectivities is a three positive spike reflectivity with each spike separated by two sample rate steps (top Figure 13). The second reflectivity created consists of five pairs of spikes increasing in separation as time increases with six minor spikes situated between the main spikes (top Figure 14). The final reflectivity is made up of a random set of spikes with random amplitudes (top

Figure 15). Each of these reflectivities is 1 second long and has 0.5 ms sample rate. Each reflectivity was convolved with the original sweep 3801 to form a new uncorrelated synthetic trace (not shown).

A total of seven correlations using TDGD calculate harmonics were conducted on each of the three uncorrelated synthetic traces. The first three correlations are so similar they appear to be coincident on Figure 13, Figure 14 and Figure 15. These three correlations include the analyzed sweep (all harmonics), H1+H2, and H1. All three of these correlations appear stacked on top of each other in C, D, and E in the correlation figures.

Harmonics H2, H3 and H4 were used as separate correlation operators and plotted on C, D, and E respectively on Figure 13, Figure 14 and Figure 15. In each figure, H2 was multiplied by 5, H3 was multiplied by 20 and H4 was multiplied by 30 to be observable on their respective plots. The reflectivity had to be multiplied by 10^13 on all plots containing correlated synthetic traces.

As can be seen on Figure 13, the three spike reflectivity remains "invisible" to the correlation using the analyzed sweep, H1+H2, and H1. The correlation using H3 (D), however, resolves the three spikes better than all other components. While H4 (E) does appear to resolve all three spikes, the amplitudes at those spikes are nearing non-uniqueness with respect to the other peaks and troughs along the trace. H2 (C) only resolves two spikes.

The increasing separation of spikes and resulting correlations in Figure 14 offers a different conclusion about harmonic resolution than its more simplified triple spike predecessor. While the correlation using H3 (D) does resolve a majority of the spikes, H2 (C) appears to have stronger amplitudes, even resolving some of the smaller spikes between the large spikes. The correlation using H4 (E), while appearing to resolve spikes, now suffers from a bad case of non-unique amplitudes.

With both positive and negative amplitudes and random placement of spikes the reflectivity presented in Figure 15 is far more realistic than the previous two reflectivities. The correlation results in Figure 15 have put yet another proverbial nail in the coffin for using H4 (E) for correlation purposes. Compared to H2 (C) and H3 (D) results, H4 correlation amplitudes appear non-unique for most spikes. With any added noise, spreading loss, and Q, H3 would most likely resolve even less of the spikes than it does now. H3 (D) correlation resolving power appears to have also decreased when faced with a random reflectivity.

The correlation results in Figure 13, Figure 14 and Figure 15 appear to show that H2 is the best harmonic to use for multiple reflecting resolving purposes. All correlations in these figures are free of spreading loss, noise and Q. However, as shown on Figure 4, the RMS power of H2 mostly exceeds the RMS power of error/noise. We can conclude from RMS power calculations (Figure 4) and correlation results that further harmonic correlation analysis can be limited to H2 as found by TDGD.

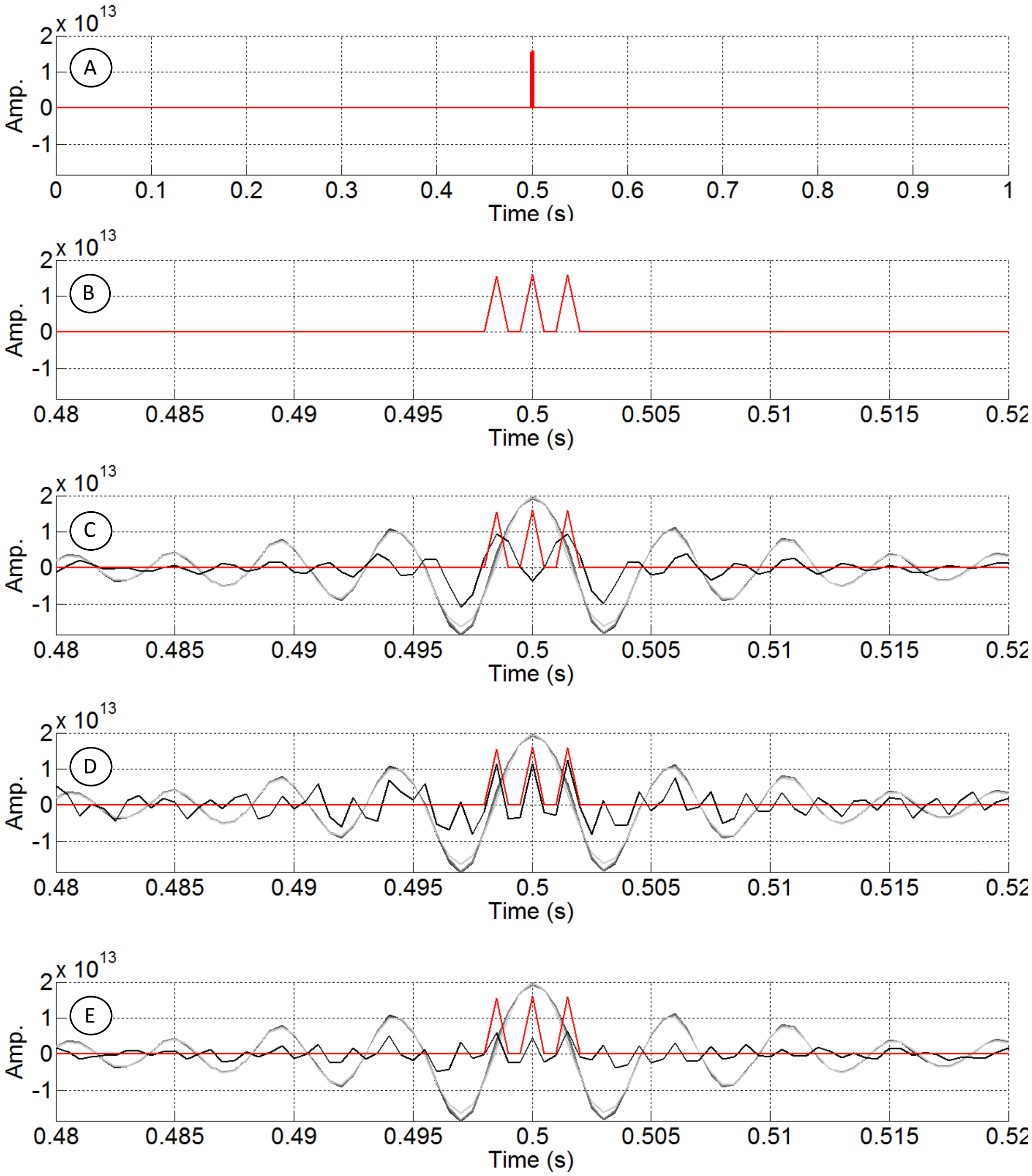

Figure 13. Three spike reflectivity as seen from its full 1 second length (A), and from a zoomed in perspective (B). Correlations which include the original sweep, analyzed sweep, H1+H2, and H2 in black (C), correlations with original, analyzed, and H3 in black (D) and correlations with original analyzed and H4 in black (E).

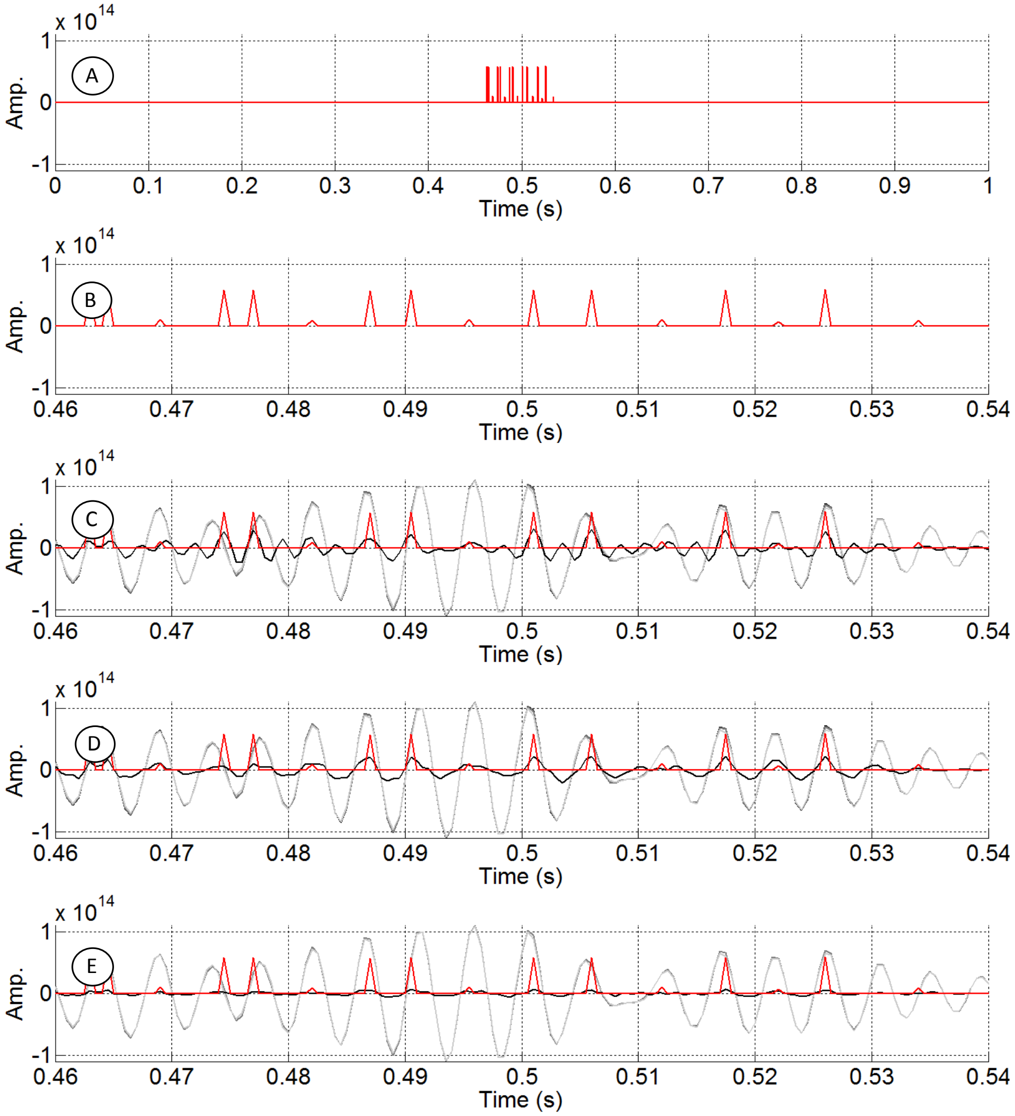

Figure 14. Five sets of spikes increasing in separation seen from its full 1 second length (A), and from a zoomed in perspective (B). Correlations which include the original sweep, analyzed sweep, and H2 in black (C), correlations with original, analyzed, and H3 in black (D) and correlations with original analyzed and H4 in black (E).

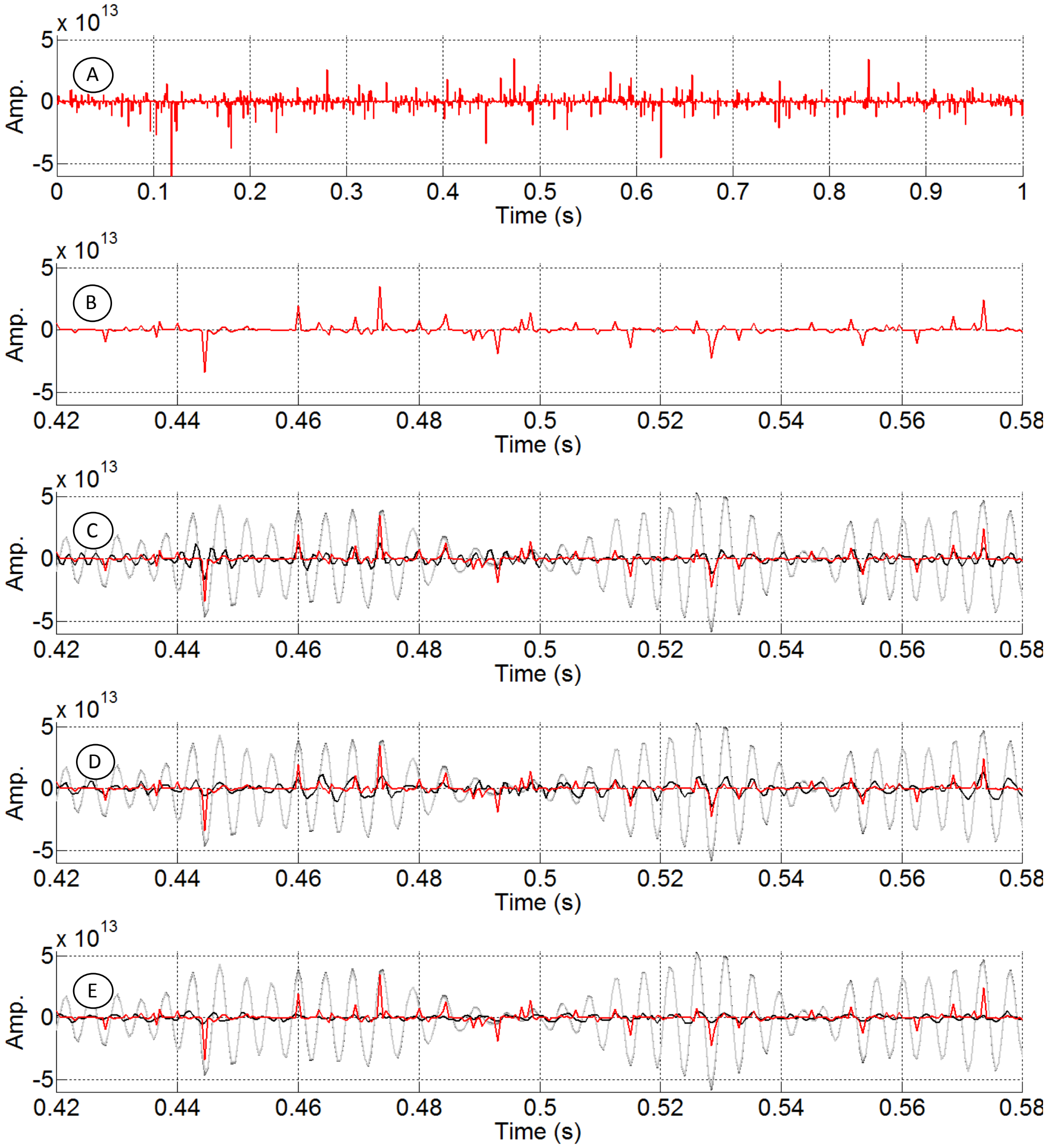

Figure 15. A random reflectivity as seen from its full 1 second length (A), and from a zoomed in perspective (B). Correlations which include the original sweep, analyzed sweep, and H2 in black (C), correlations with original, analyzed, and H3 in black (D) and correlations with original analyzed and H4 in black (E).

Field Data

To this point we have been dealing in the realm of synthetic data free of noise, spreading loss and Q. The field data we are going to use are the same data from which our test sweep, 3801, was gleaned. This survey contains 1877 shot points using 192 geophones at 3 meter intervals. Non-linear 6-240 Hz 20 second long sweeps were shot every 12 meters along an iced road. Table 1 contains the sweep and acquisition parameters for quick reference.

Table 1. Sweep and survey parameters.

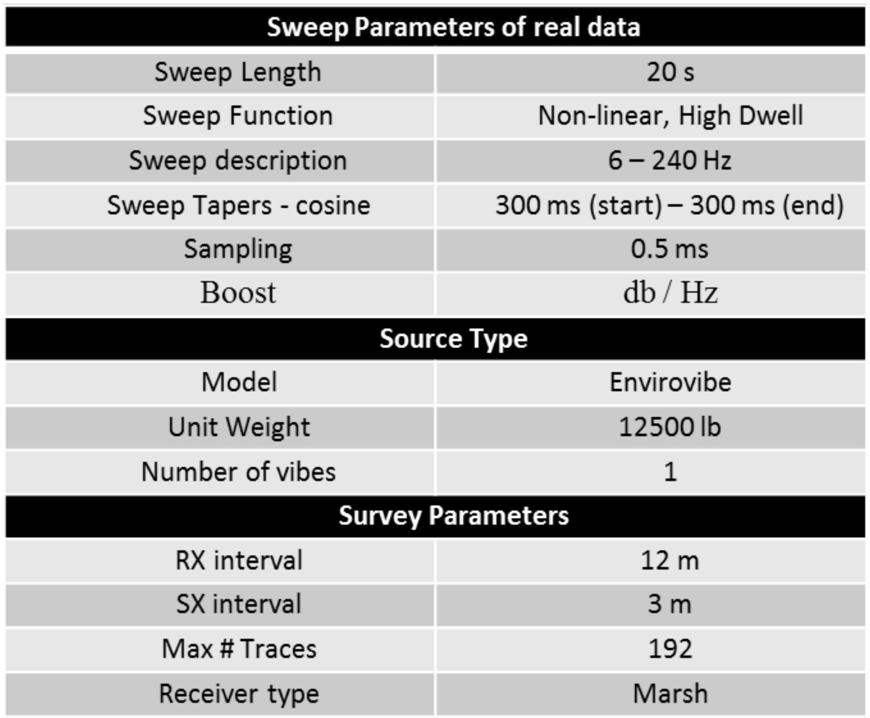

Sweep Parameters of real data	
Sweep Length	20 s
Sweep Function	Non-linear, High Dwell
Sweep description	6 – 240 Hz
Sweep Tapers - cosine	300 ms (start) – 300 ms (end)
Sampling	0.5 ms
Boost	db / Hz
Source Type	
Model	Envirovibe
Unit Weight	12500 lb
Number of vibes	1
Survey Parameters	
RX interval	12 m
SX interval	3 m
Max # Traces	192
Receiver type	Marsh

The field data was recorded un-correlated, allowing us to correlate with any operators we choose. Time constraints have limited us to using only the pilot sweep and the TDGD H2 as correlation operators.

Processing Flow

The field data were processed in two separate flows using the industry standard pilot sweep and the TDGD H2 as the correlation operators. A basic processing flow in Table 2 below shows how each data set was handled. The correlation using the pilot sweep was the first flow. Geometry, final velocity and final residual statics for the pilot correlation were also used for the H2 correlation. The final pilot correlated processed seismic image to 1000 ms is shown in Figure 16. Geological periods are annotated on the left of the image with key horizons and formations annotated on the right. The final H2 correlated processed seismic image to 1000 ms is shown in Figure 17. The same annotation is shown on Figure 17 as in Figure 16.

Table 2. Basic processing flow for correlation using the pilot sweep

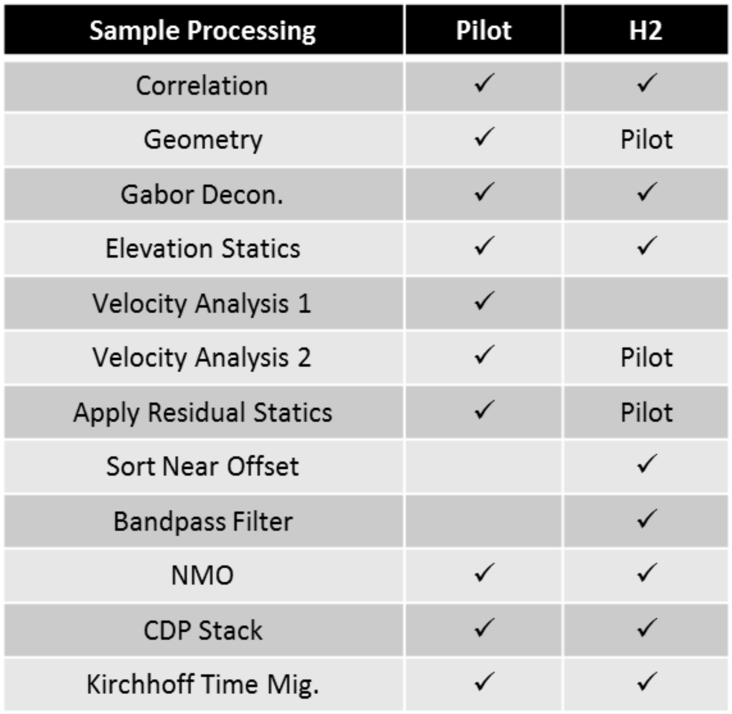

Sample Processing	Pilot	H2
Correlation	✓	✓
Geometry	✓	Pilot
Gabor Decon.	✓	✓
Elevation Statics	✓	✓
Velocity Analysis 1	✓	
Velocity Analysis 2	✓	Pilot
Apply Residual Statics	✓	Pilot
Sort Near Offset		✓
Bandpass Filter		✓
NMO	✓	✓
CDP Stack	✓	✓
Kirchhoff Time Mig.	✓	✓

There are several key differences between the pilot correlated processing of Figure 16 and the H2 correlated processing of Figure 17. The higher frequencies of H2 have been attenuated much faster through the ground, resulting in the “washed out” appearance below 250 ms on Figure 17. The lower frequencies of the pilot correlated processed image, as expected, show a clear advantage for deeper imaging. The bonus to this “washed out” lower section of the H2 image is the obvious increase in possible reflector imaging in the upper 250ms.

Far more detail can be observed through the Quaternary channel and fill between 25 and 125 ms on Figure 17. The base of this channel fill, varying between 100 and 125 ms, appears to have many more layers in Figure 17 than its lower frequency counterpart in Figure 16. Further, the upper section of this channel fill between 50 to 100 ms, appears to also have more reflections in the H2 correlated image. However, some of the layers in this fill formation do match on both the pilot and H2 correlated images. These similarities provide us with at least a good degree of confidence that our processing flows are compatible.

Another important feature between our two images is the “booming” Viking horizon at 175 ms on Figure 16 which is not so “booming” on the high frequency image in Figure 17. The Viking Formation appears to have more layering associated with it in Figure 17, but is also more difficult to delineate across the seismic image. These “extreme” differences between the two images show the delineation advantage of the pilot correlated processed seismic data.

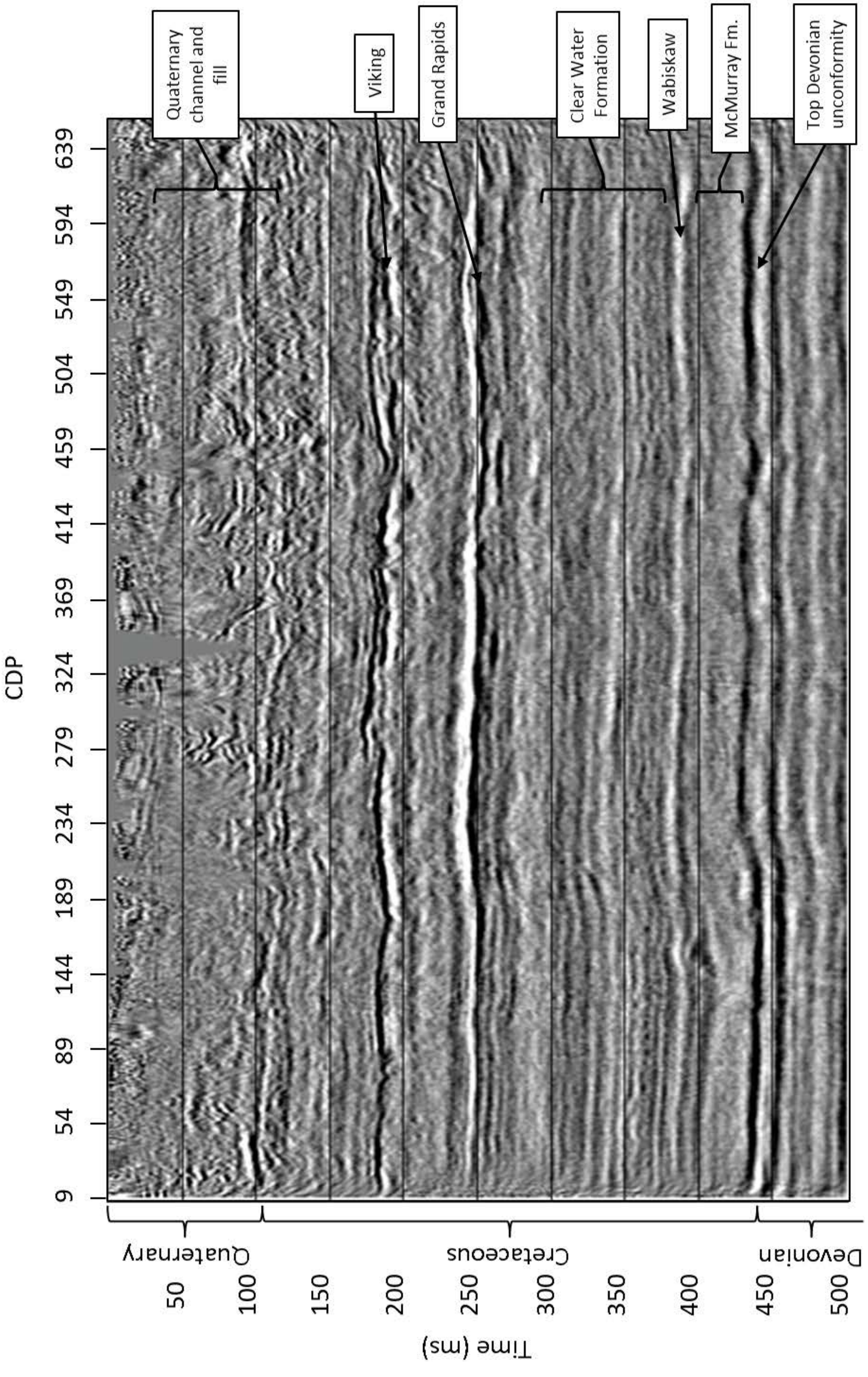

Figure 16. The pilot sweep correlated processed seismic image with annotation.

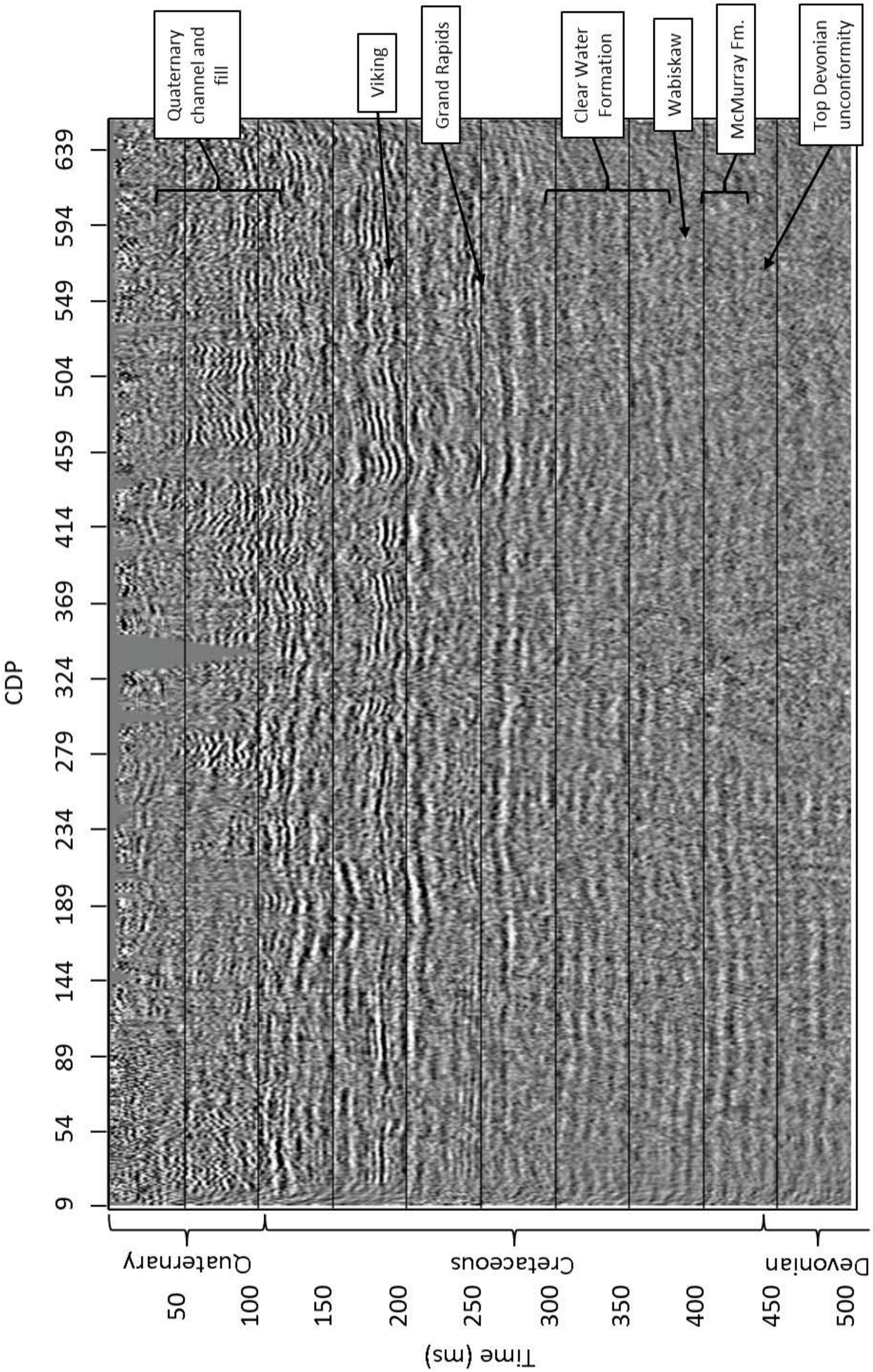

Figure 17. The TDGD H2 sweep correlated processed seismic image with annotation.

Conclusions

Harmonics generated by the vibrator have traditionally been seen as noise to be attenuated out of the sweeps and traces during the acquisition and seismic data processing phases. We have shown in our research, however, that the higher harmonic frequencies can be harnessed for imaging shallow thin reflectors.

Our initial synthetic studies showed overwhelmingly that correlation using higher order harmonics better imaged closer spaced reflectors. The second and third harmonic acquired through TDGD and FDGD both appeared to provide the best synthetic correlation results for imaging. However, these synthetic results were free of spreading loss, noise and Q. We next correlated field data with both a pilot sweep and the TDGD H2 to observe the differences between the two correlation operators. The final processed images showed that using H2 as the correlation operator revealed more reflections in the near surface than the pilot correlated data.

There is still much research to be done, but our results thus far provide a very compelling case for harnessing harmonics for imaging instead of attenuating them out of the equation.

Future Work

- Doubling pilot sweep as H2
- Correlation with H1+H2, and H3
- Use of ground force and its harmonics as correlation operator.
- Investigate phase of the harmonics. If they are not in phase, we have to find out how to make them in phase.

References

Abd El-Aal, A. E. K. (2011). "Harmonic by harmonic removal technique for improving vibroseis data quality." Geophysical Prospecting(59): 279-294.

Bagaini, C. (2006). Overview of simultaneous Vibroseis acquisition methods. SEG Annual Meeting. New Orleans, SEG**:** 70-74.

Bagaini, C. (2010). "Acquisition and processing of simultaneous vibroseis data." Geophysical Prospecting **58**: 81-99.

Benabentos, M., Ortigosa, F., Moldoveanu, N., and Munoz, P. (2006). "Cascaded sweeps - A method to improve vibroseis acquisition efficiency: A field test." The Leading Edge **June**(693-697).

Beresnev, I. A. (2012). "Ground-force- or plate-displacement-based vibrator control?" Journal of Sound and Vibrations(331): 1715-1721.

Dal Moro, G., Scholtz, P. and Iranpour, K. (2007). Harmonic noise attenuation for Vibroseis data. GNGTS – 26°. C. Nazionale.

Eisner, E. (1974). Method for determining optimum seismic pulse. US Patent. **3,815,704**.

Harrison, C. B., Margrave, Gary F., Lamoureux, Michael P., Siewert, Arthur, Barrett, Andrew (2011). "Harmonic decomposition of vibroseis sweeps using Gabor analysis." CREWES Research Report **2011**.

Lebedev, A. V., and Beresnev, I. A. (2004). "Nonlinear distortions of signals radiated by vibroseis sources." Geophysics **69**(4): 968-977.

Li, X. P. (1997). "Decomposition of vibroseis data by the multiple filter technique." Geophysics **62**(3): 980-991.

Li, X. P., Sollner, W., and Hubral, P. (1995). "Elimination of harmonic distortion in vibroseis data." Geophysics **60**(2): 503-516.

Martin, J. E. (1993). "Simultaneous vibroseis recording." Geophysical Prospecting **41**: 943-967.

Martin, J. E., White, R.E. (1989). "Two methods for continuous monioring of harmonic distortion in vibroseis signals." Geophysical Prospecting **37**: 851-872

Moerig, R., Barr, F.J., Nyland, D.L., and Sitton, G. (2004). Method of using cascaded sweeps for source coding and harmonic cancellation. U. Patent. US. **6,687,619**.

Okaya, A. D., Karageorgi, E., McEvilly, T. V., and Malin, P. E. (1992). "Removing vibrator induced correlation artifacts by filtering in frequency-uncorrelated time space." Geophysics **57**: 916-926.

Polom, U. (1997). "Elimination of source-generated noise from correlated vibroseis data (the 'ghost-sweep' problem)." Geophysical Prospecting **45**: 571-591.

Rietsch, E. (1981). "Reduction of harmonic distortion in vibratory source records." Geophysical Prospecting **29**: 178-188.

Rozemond, H. J. (1996). Slip-sweep acquisition. SEG meeting. Denver, Colorado, USA, SEG. **Extended Abstracts:** 64-67.

Schrodt, J. K. (1987). "Techniques for improving Vibroseis data." Geophysics **52**: 469-482.

Sercel (2010). 428XL User's Manual Sercel. **1:** 470-472.

Seriff, A. J., and Kim W.H. (1970). "The effect of harmonic distortion in the use of vibratory surface sources." Geophysics **35**(2): 234-246.

Silverman, D. (1979). Method of three dimensional seismic prospecting. U.S. Patent. **4,159,463**.

Sorkin, S. A. (1972). Sweep signal seismic exploration U.S. Patent. **3,786,409**.

Walker, D. (1995). "Harmonic resonance structure and chaotic dynamics in the earth-vibrator system." Geophysical Prospecting **43**: 487-507.

Wei, Z., and Hall, M.A. (2011). "Analyses of vibrator and geophone behavior on hard and soft ground." The Leading Edge **Feb**: 132-137.